The C terminus of the mycobacterium ESX-1 secretion system substrate ESAT-6 is required for phagosomal membrane damage and virulence

Morwan M. Osman, Jonathan K. Shanahan, Frances Chu, Kevin K. Takaki, Malte L. Pinckert, Antonio J. Pagán, Roland Brosch, William H. Conrad, Lalita Ramakrishnan

The C terminus of the mycobacterium ESX-1 secretion system substrate ESAT-6 is required for phagosomal membrane damage and virulence

Morwan M. Osman[a,b,1,2], Jonathan K. Shanahan[a,b,1], Frances Chu[c,3], Kevin K. Takaki[a,b], Malte L. Pinckert[a,b,4], Antonio J. Pagán[a,b] , Roland Brosch[d] , William H. Conrad[a,b,5] , and Lalita Ramakrishnan[a,b,c,6]

[a]Molecular Immunity Unit, Cambridge Institute of Therapeutic Immunology and Infectious Diseases, Department of Medicine, University of Cambridge, CB2 0QH Cambridge, United Kingdom; [b]Cell Biology Division, Medical Research Council Laboratory of Molecular Biology, CB2 0QH Cambridge, United Kingdom; [c]Department of Microbiology, University of Washington, Seattle, WA 98105; and [d]Institut Pasteur, Université de Paris, CNRS UMR 3525, Unit for Integrated Mycobacterial Pathogenomics, 75724 Paris Cedex 15, France

Mycobacterium tuberculosis and its close relative *Mycobacterium marinum* infect macrophages and induce the formation of granulomas, organized macrophage-rich immune aggregates. These mycobacterial pathogens can accelerate and co-opt granuloma formation for their benefit, using the specialized secretion system ESX-1, a key virulence determinant. ESX-1–mediated virulence is attributed to the damage it causes to the membranes of macrophage phagosomal compartments, within which the bacteria reside. This phagosomal damage, in turn, has been attributed to the membranolytic activity of ESAT-6, the major secreted substrate of ESX-1. However, mutations that perturb ESAT-6's membranolytic activity often result in global impairment of ESX-1 secretion. This has precluded an understanding of the causal and mechanistic relationships between ESAT-6 membranolysis and ESX-1–mediated virulence. Here, we identify two conserved residues in the unstructured C-terminal tail of ESAT-6 required for phagosomal damage, granuloma formation, and virulence. Importantly, these ESAT-6 mutants have near-normal levels of secretion, far higher than the minimal threshold we establish is needed for ESX-1–mediated virulence early in infection. Unexpectedly, these loss-of-function ESAT-6 mutants retain the ability to lyse acidified liposomes. Thus, ESAT-6's virulence functions in vivo can be uncoupled from this in vitro surrogate assay. These uncoupling mutants highlight an enigmatic functional domain of ESAT-6 and provide key tools to investigate the mechanism of phagosomal damage and virulence.

ESAT-6 | ESX-1 | phagosomal damage | virulence

The type VII secretion system ESX-1 (ESAT-6 secretion system 1) is a major virulence determinant in *Mycobacterium tuberculosis* (Mtb) and its close relative *Mycobacterium marinum* (Mm) (1–4). ESX-1 was identified as a virulence determinant when a 9.4-kb deletion in this region was discovered in the live attenuated tuberculosis vaccine Bacillus Calmette–Guérin (BCG) (2, 5). This "region of difference 1 (RD1)" was found to be required for both Mtb and Mm virulence (1, 2). The *esx-1* locus was then found to extend beyond RD1 in both organisms (6, 7) (*SI Appendix*, Fig. S1A). Mtb and Mm ESX-1 systems are functionally equivalent: complementation of Mm−ΔRD1 with a cosmid containing the Mtb ESX-1 locus restores ESX-1 functions (8), and the use of Mm has facilitated fundamental discoveries about ESX-1 function (9). ESX-1 promotes virulence through an array of processes, including activation of cytosolic signaling pathways, macrophage death, and pathogenic acceleration of tuberculous granulomas through induction of MMP9, which in turn promotes mycobacterial growth (3, 9–12). ESX-1 also mediates damage of the macrophage phagosomal membranes in which the bacteria reside, and this is thought to be integral to ESX-1–mediated virulence (13–15).

ESX-1's membranolytic activity had been ascribed to its major secreted substrate ESAT-6 (6 kDa early secretory

antigenic target) (16). ESAT-6 was discovered as a secreted, immunodominant Mtb antigen long before the *esx-1* locus was identified (17). Once the *esx-1* locus was identified, it was determined that the genes encoding ESAT-6 (*esxA*) and its secreted partner CFP-10 (*esxB*) reside in RD1 (*SI Appendix*, Fig. S1A) (5, 6). ESAT-6 and CFP-10 (95 and 100 amino acids, respectively), were the first identified members of the type VII secretion-associated WXG100 superfamily, so named for their conserved WXG motif and their size of ~100 amino acids (18). Pinning down the role of ESAT-6 and other ESX-1 substrates in membranolysis and virulence has been complicated by their codependency for secretion, as deletion of ESAT-6 abrogates secretion of other ESX-1 substrates (19, 20). A separate line of

Significance

Tuberculosis (TB), an ancient disease of humanity, continues to be a major cause of worldwide death. The causative agent of TB, *Mycobacterium tuberculosis*, and its close pathogenic relative *Mycobacterium marinum*, initially infect, evade, and exploit macrophages, a major host defense against invading pathogens. Within macrophages, mycobacteria reside within host membrane–bound compartments called phagosomes. Mycobacterium-induced damage of the phagosomal membranes is integral to pathogenesis, and this activity has been attributed to the specialized mycobacterial secretion system ESX-1, and particularly to ESAT-6, its major secreted protein. Here, we show that the integrity of the unstructured ESAT-6 C terminus is required for macrophage phagosomal damage, granuloma formation, and virulence.

MICROBIOLOGY

evidence used purified recombinant ESAT-6 to implicate it in membranolysis. Purified ESAT-6, but not its cosecreted partner CFP-10, lysed artificial lipid bilayers, liposomes, and red blood cells (RBCs), leading to the conclusion that ESAT-6 functions as a classical pore-forming toxin (15, 21, 22).

However, we and others found that many of the pore-forming activities ascribed to ESAT-6, such as RBC lysis, was due to residual detergent contamination in ESAT-6 preparations made using standard, widely distributed protocols (8, 23, 24). Moreover, we found that true ESX-1–mediated RBC lysis was contact dependent and caused gross membrane disruptions as opposed to distinct pores (8). These findings suggested that ESAT-6 was either not directly involved in ESX-1–mediated membranolysis in vivo or required additional mycobacterial factors. One such additional factor has been identified: We and others have shown that the mycobacterial cell surface lipid phthiocerol dimycocerosate (PDIM) is also required for macrophage phagosomal damage in both Mtb and Mm (25–29). There is also increasing evidence that ESX-1 substrates other than ESAT-6 are required for its pathogenic activity. Mm mutants in the ESX-1 genes *espE* and *espF* secrete normal levels of ESAT-6 but are attenuated in ESX-1–mediated virulence functions (30). These findings suggest that ESAT-6 is not sufficient for the ESX-1 virulence function, while leaving open the question of whether it is necessary. Continued efforts to understand to what extent ESAT-6 is directly involved in ESX-1 membranolysis and virulence have not provided clear answers. Mm transposon mutants have been identified that do not secrete ESAT-6 but are capable of damaging macrophage phagosomes as evidenced by bacterial cytosolic translocation (31), and ESAT-6 secretion-deficient ESX-1 mutants have been identified that are unaffected in intramacrophage growth and/or virulence in Mm and Mtb (32–36). These findings go against a direct role for ESAT-6 in ESX-1's membranolytic activity. However, there is also strong evidence supporting ESAT-6's direct involvement in ESX-1–mediated membranolytic activity and virulence. Levels of surface-bound ESAT-6 correlate with cytotoxicity and intramacrophage growth (35, 37). An N-terminal ESAT-6 point mutation (Q5K) preserves ESAT-6 secretion but attenuates phagosomal permeabilization, cytotoxicity, and Mm growth in cultured macrophages and zebrafish larvae (38). Covalent modification of secreted ESAT-6 reduces hemolysis and intramacrophage growth (39), suggesting that ESAT-6 functions as a secreted effector. ESAT-6 Q5K and covalently modified ESAT-6 are both attenuated in ability to lyse acidified liposomes, which is considered a proxy for its in vivo membranolytic activity. Lysis of acidified liposomes is the single in vitro assay where both recombinant and natively purified Mtb ESAT-6 exhibit membranolytic activity in the absence of contaminating detergent (21, 23, 40).

In this work, we probe the role of ESAT-6 in virulence. We find that mutation of EccA1, a putative ESX-1 chaperone, or treatment with the drug ebselen results in drastic reduction in secretion of ESAT-6 and its cosecreted partner, CFP-10. Both the *eccA1* mutant and ebselen-treated Mm retain substantial phagosome-damaging activity, growth, and granuloma formation in vivo. In contrast, we find that two C-terminal point mutations in ESAT-6 allow substantial levels of ESAT-6 and CFP-10 secretion but cause complete loss of phagosomal membrane damage and virulence. Moreover, mutation of the C terminus still allows for lysis of acidified liposomes, showing that there are additional requirements for ESAT-6–mediated membrane damage in vivo.

Results

Minimal ESAT-6 Secretion Suffices for ESX-1's Pathogenic Functions.
In prior work, we found that a C-terminal M93T point mutation in ESAT-6 (Mm−ΔRD1::M93T$_{mt}$) resulted in greatly decreased secretion not only of ESAT-6, but also of CFP-10 (8). As CFP-10

is dependent on ESAT-6 for secretion, this suggested that the mutation might disrupt ESX-1 virulence simply by compromising ESAT-6–dependent ESX-1 substrate secretion (8). However, Mm mutants in *eccA1*, which encodes the EccA1 AAA+ ATPase—a putative chaperone for ESX-1 substrates—are also deficient for ESAT-6 and CFP-10 secretion (7, 33); yet, they are reported to be only somewhat compromised for virulence (33, 36). This suggested that minimal ESAT-6 secretion is sufficient for ESX-1–mediated virulence. To study the link between ESAT-6 secretion and ESX-1–mediated virulence phenotypes, we examined a Mm transposon mutant in *eccA1* (Mm-*eccA1*::Tn). We confirmed that Mm-*eccA1*::Tn had minimal ESAT-6 and CFP-10 secretion, comparable to that of Mm−ΔRD1::M93T$_{mt}$ (Fig. 1*A* and see Fig. 3*B*) (8). We also confirmed that Mm-*eccA1*::Tn was deficient for RBC lysis, as previously reported (Fig. 1*B*) (7, 33). Next, we examined the extent to which Mm-*eccA1*::Tn could damage phagosomal membranes by using the galectin-8 staining assay. This assay takes advantage of the fact that cytosolic galectins bind to luminal β-galactoside–containing glycans that become exposed on damaged vesicles and can be visualized by immunofluorescence microscopy (Fig. 1*C*) (28, 41, 42). Infection with Mm-*eccA1*::Tn resulted in decreased galectin-8 puncta but substantially more than an Mm−ΔRD1 (26% vs. 7% of wild-type puncta) (Fig. 1*D*). Also, as previously reported, Mm-*eccA1*::Tn had only partially attenuated growth in cultured macrophages (Fig. 1*E*) (7, 33). It achieved nearly wild-type bacterial burdens during zebrafish larval infection (0.82 ± 0.16 fold of wild type vs. 0.29 ± 0.05 fold for Mm−ΔRD1), and this was associated with wild type levels of granuloma formation, an ESX-1–mediated phenotype (Fig. 1 *F–H*) (3, 11, 12). Thus, the reduction in ESAT-6 secretion resulting in *eccA1*::Tn abrogates RBC lysis but retains significant phagosome-damaging activity and nearly wild-type levels of growth in human and zebrafish macrophages, at least over the first few days of infection.

To further investigate the relationship between levels of ESAT-6 secretion, membranolysis, and virulence, we used the drug ebselen. Ebselen reduces ESAT-6 secretion in wild-type Mm to similar levels as Mm-*eccA1*::Tn albeit through an EccA1-independent mechanism (43). Ebselen resulted in the same dissociation between ESAT-6 secretion and virulence phenotypes in wild-type Mm that we had observed for Mm-*eccA1*::Tn, with inhibition of RBC lysis and phagosomal damage combined with a minimal effect on intracellular bacterial growth (Fig. 1 *I–K*). Zebrafish experiments with ebselen were precluded by drug toxicity at concentrations exceeding 1 μM, a dose at which ebselen shows no effect on ESX-1 function (43). In sum, minimal ESAT-6 secretion is sufficient to support some level of phagosomal damage, which, in turn, is sufficient for substantial mycobacterial virulence at least early in infection. Given this insight, the reduction in ESX-1 substrate secretion in Mm−ΔRD1::M93T$_{mt}$ was not sufficient to explain its complete loss of phagosomal damage and virulence, warranting further investigation of the role of ESAT-6 and, particularly, its C terminus.

ESAT-6 C-Terminal Point Mutants Retain Appreciable ESAT-6 Secretion.
Residues 83 to 95 of ESAT-6 form a highly conserved C-terminal motif (Fig. 2 *A–C* and *SI Appendix*, Fig. S3) (44). Our prior work on the effect of the ESAT-6 M93T mutation had used an RD1 deletion mutant of Mm complemented with a cosmid encoding the Mtb extended ESX-1 region with an ESAT-6 M93T point mutation (Mm−ΔRD1::M93T$_{Mtb}$) (Fig. 2 *A–C* and *SI Appendix*, Fig. S1). For a more refined analysis, we constructed an ESAT-6 deletion mutant (Mm−Δ*esxA*) and complemented it using an integrating plasmid expressing wild-type ESAT-6 or an ESAT-6 M93T point mutant (*SI Appendix*, Fig. S1). We also generated a second ESAT-6 point mutant in
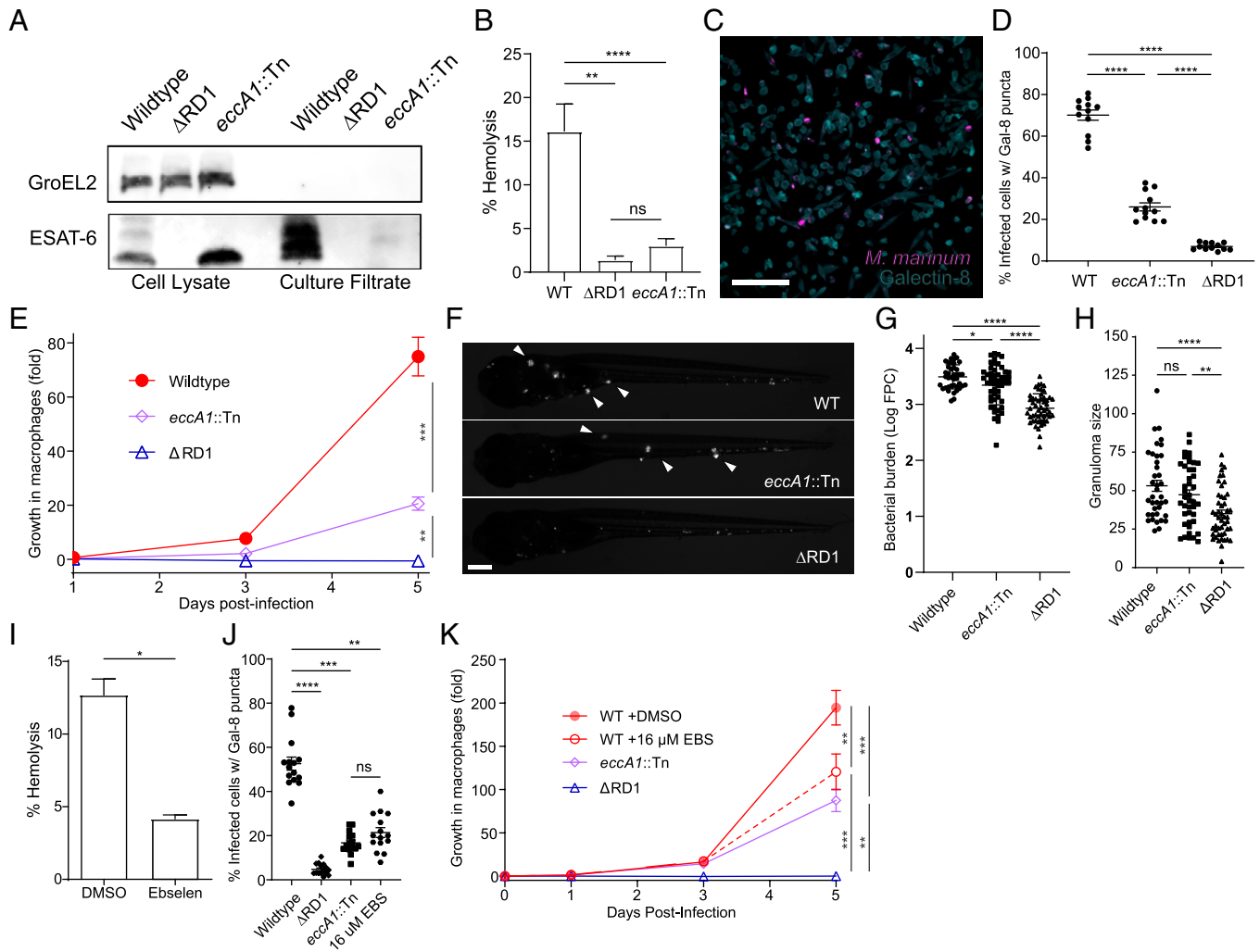
Fig. 1. Minimal ESX-1 secretion is required for intramacrophage survival and virulence. (*A*) Immunoblot of 48-h Mm cell lysates and culture filtrates. Data are representative of three independent experiments. GroEL2 is shown as a lysis control. (*B*) Contact-dependent hemolysis of RBCs by Mm. Data are combined from four experimental replicates. (*C*) Representative image of THP-1 cells infected with Mm, stained for galectin-8. (Scale bar, 100 μm.) (*D*) Percent of infected THP-1 macrophages with galectin-8 puncta. Each data point represents an individual imaging field. Horizontal lines, means. Statistics: One-way ANOVA with Šidák's multiple comparisons test. (*E*) Intramacrophage growth of Mm within J774A.1 cells as measured by bacterial fluorescence. Data are representative of three independent experiments. (*F–H*) Zebrafish larvae at 5 d postinfection. Data are representative of four independent experiments. (*F*) Representative images. (Scale bar, 250 μm.) Arrowheads, granulomas. (*G*) Bacterial burdens as assessed by bacterial fluorescence. (*H*) Average infection foci size per larva. Statistics: One-way ANOVA with Dunnett's test. (*I*) Contact-dependent hemolysis of RBCs by Mm treated with vehicle or 16 μM ebselen. Data are combined from four experimental replicates. (*J*) Percent of infected THP-1 macrophages with galectin-8 puncta. Each data point represents an individual imaging field. Horizontal lines, means. Statistics: One-way ANOVA with Šidák's multiple comparisons test. (*K*) Intramacrophage growth of J774A.1 cells infected with Mm. Data are representative of three independent experiments. (*E* and *K*) One-way ANOVA with Bonferroni's multiple comparisons test. Statistics: ****$P < 0.0001$, ***$P ≤ 0.001$, **$P < 0.01$, *$P < 0.05$; not significant (ns), $P > 0.05$. WT, wild type.

both ESX-1 and ESAT-6 complementation systems, altering another highly conserved methionine to an isoleucine Mm−ΔRD1::M83I_{Mtb} and Mm−Δ*esxA*::M83I_{Mtb} (Fig. 2 *A–C*). We found that Mm−ΔRD1::M83I_{Mtb} behaved similarly to Mm−ΔRD1::M93T_{Mtb}, displaying reductions in secretion and intramacrophage growth (*SI Appendix*, Fig. S2) (8, 45).

We found that Mm−Δ*esxA* had total loss of ESAT-6 and CFP-10 secretion, similar to Mm−ΔRD1, and this was restored by *esxA* complementation (Fig. 3*A*). Complementation of Mm−Δ*esxA* with ESAT6 M93T (Δ*esxA*::M93T_{Mtb}) restored secretion to a substantial degree, more than the original cosmid complementation system and much more than Mm-*eccA1*::Tn (Fig. 3 *A* and *B*). Thus, the reduced secretion seen with the cosmid complementation of Mm−ΔRD1 is likely an artifact of partial complementation of the RD1 locus, gene dosage effects, subunit stoichiometry effects, or a combination of these that

are mitigated by the current system. Importantly, the two C-terminal mutations largely preserve ESAT-6 and CFP-10 secretion.

ESAT-6 C-Terminal Point Mutants Lose Membranolytic Activity and Virulence. We could now use the two mutants to study the impact of ESAT-6 C-terminal integrity on ESAT-6 membranolytic activity and virulence. We first ascertained that Mm−Δ*esxA* was compromised for RBC lysis activity, phagosomal damaging activity, macrophage growth, and growth and granuloma formation in zebrafish larvae, similar to Mm−ΔRD1 (Fig. 4 *A–F*) (8, 11, 28). All of these defects were rescued by complementation with Mtb ESAT-6 (Mm−Δ*esxA*::WT_{Mtb}) (Fig. 4 *A–F*). However, ESAT-6 bearing either C-terminal mutation failed to complement any of the phenotypes. Thus, the integrity of the ESAT-6 C terminus, while largely dispensable for
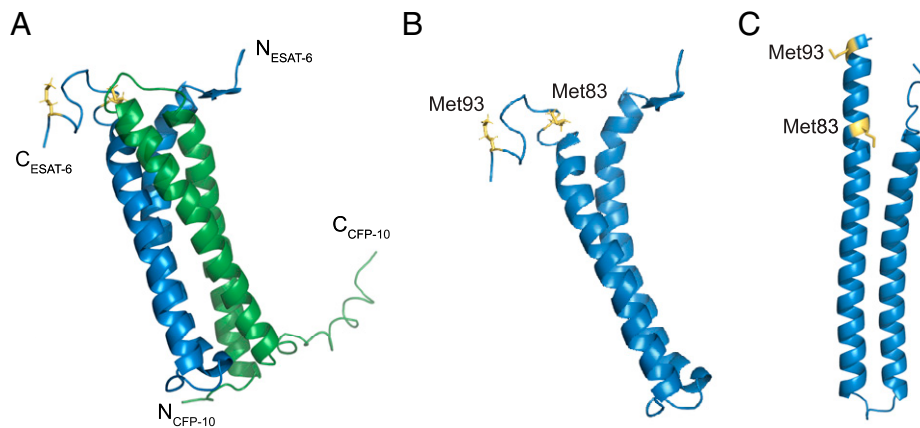
Osman et al.
The C terminus of the mycobacterium ESX-1 secretion system substrate ESAT-6 is required for phagosomal membrane damage and virulence

PNAS | 3 of 9
https://doi.org/10.1073/pnas.2122161119

MICROBIOLOGY

Fig. 2. ESAT-6 structures with C-terminal point mutations. (*A*) NMR structure of the heterodimer formed by ESAT-6 (blue) and CFP-10 (green) (Protein Data Bank [PDB] 1WA8). N and C termini of ESAT-6 and CFP-10 are as labeled, as well as methionine 83 and 93 of ESAT-6 (yellow). (*B* and *C*) Structure of ESAT-6 alone with methionine residues 83 and 93 highlighted, as determined experimentally by NMR (*B*) or by the predicted model using AlphaFold2 (*C*).

secretion, is absolutely required for phagosomal membrane damage, which, in turn, is linked to granuloma formation and mycobacterial growth in vivo.

The ESAT-6 M93T Mutant Retains Wild-Type Levels of Acidified Liposome Lysis Activity. Under acidic conditions (≤pH 5), ESAT-6 undergoes a conformational shift and inserts into liposomal membranes, resulting in their lysis (16, 46). Based on these observations, ESAT-6's lysis of acidified liposomes has been used as a proxy for its role in phagosomal damage and permeabilization (16, 23). However, the relevance of the liposome lysis assay for ESAT-6's role in phagosomal damage has been unclear. During Mm and Mtb infection, inhibition of phagosomal acidification using the vacuolar type ATPase (V-ATPase) inhibitors, bafilomycin A1 or concanamycin A, either has no effect on or even enhances phagosomal permeabilization/damage (8, 26, 47, 48). However, it has been argued that these findings may represent artifacts caused by alterations in phagosomal membrane composition caused by chemical inhibition of V-ATPase (49). To address the role of phagosomal acidification under natural conditions, we took advantage of the observation that during macrophage infection, mycobacteria reside in both acidified and nonacidified phagosomes (50). We found that 24 h postinfection, 89% of Mm (415/469) were in acidified phagosomes as determined by staining with LysoTracker, an acidophilic dye that labels lysosomal compartments (50). Costaining with galectin-8 showed that a significantly higher proportion of bacteria residing in acidified phagosomes were positive (2-fold increase over nonacidified) (Fig. 5). To see whether phagosomal acidification also increases Mtb-mediated phagosomal damage, we used the auxotrophic Mtb H37Rv strain, mc²6206, a containment level 2 organism, which retains ESX-1 function (43, 51, 52). After 24 h, 67% (320/475) of the bacterial phagosomes were acidified. As with Mm, there was a significant

increase in galectin-8 recruitment to bacteria residing in acidified compartments (1.7-fold increase over nonacidified) (Fig. 5). These findings show that both Mm and Mtb ESAT-6–mediated phagosomal damage is indeed enhanced by acidification.

Importantly, these findings reenforced the argument that the lytic activity of ESAT-6 on acidified liposomes is a proxy of ESAT-6–mediated phagosomal damage (16). Our finding that the C-terminal mutants had almost no phagosomal damage (Fig. 4*B*), when most of the bacteria are in acidified phagosomes, indicated that they are unable to damage phagosomes even under the sensitizing acidified condition. Therefore, we expected that the C-terminal mutations would cause ESAT-6 to lose acidified liposome lysis activity. We used recombinant ESAT-6 M93T, a less conservative mutation than M83I, which we hypothesized to be more likely to disrupt ESAT-6 function. To measure lysis, we generated 1,2-dioleoyl-*sn*-glycero-3-phosphocholine (DOPC) liposomes containing the fluorescent dye 8-aminonaphthalene-1,3,6-trisulfonic acid (ANTS), a formulation which has been used for previous systematic analyses of ESAT-6's lytic activity (46, 53). We were surprised to find that ESAT-6 M93T retained wild-type levels of acidified liposome lysis (Fig. 6). This stood in contrast to findings with an N-terminal ESAT-6 point mutation (Q5K), which decreased both phagosomal damage by Mm and liposome lysis by recombinant protein (38). Thus, our finding uncouples ESAT-6's in vitro and in vivo membrane-damaging activities even under acidified conditions, suggesting an in vivo role for specific residues in the C terminus.

Discussion

This work was instigated by our finding that barely detectable levels of ESAT-6 secretion in both an Mm *eccA1* mutant and ebselen-treated Mm only halved ESX-1–mediated phagosomal
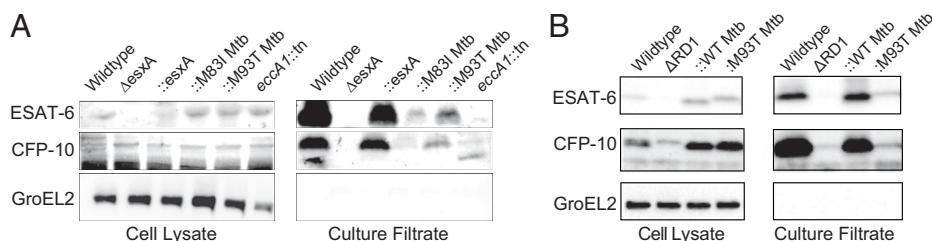

Fig. 3. C-terminal point mutations in ESAT-6 support substantial levels of ESAT-6 and CFP-10 secretion. Immunoblots of 48-h cell lysates and culture filtrates of (*A*) Mm−Δ*esxA* and (*B*) Mm−ΔRD1 mutants. Each panel representative of three independent experiments. *B* is reprinted with permission from ref. 8.
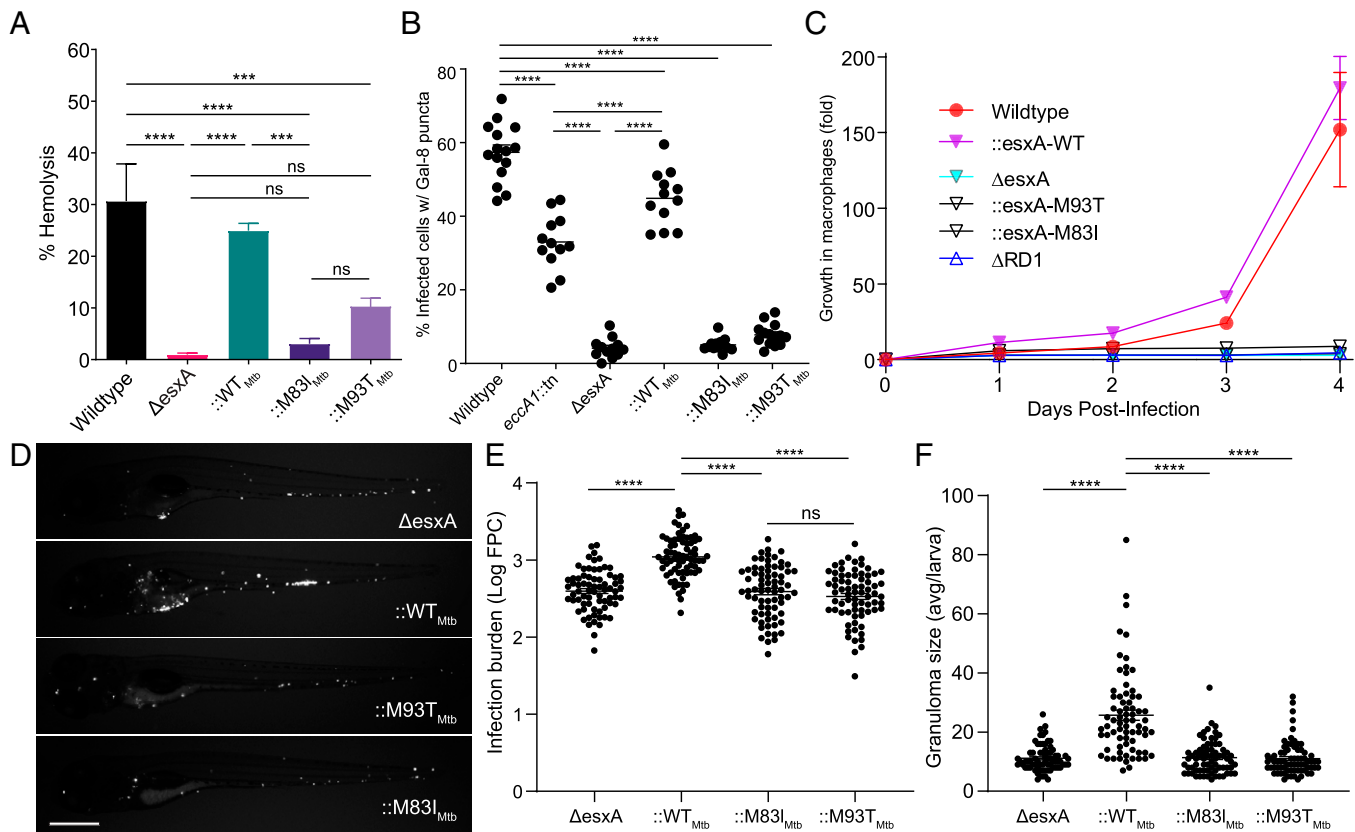
Fig. 4. ESAT-6 mediates phagosomal damage and virulence. (*A*) Contact-dependent hemolysis of RBCs by Mm. Data are combined from four experimental replicates. (*B*) Percent of infected THP-1 macrophages with galectin-8 puncta. Each data point represents individual imaging fields. Horizontal lines, means. Statistics: one-way ANOVA with Šidák correction for multiple comparisons. (*C*) Intramacrophage growth of Mm within J774A.1 macrophages as measured by bacterial fluorescence. Data are representative of four independent experiments. (*D*–*F*) Zebrafish larvae at 5 dpi. (*D*) Representative images. (Scale bar, 500 μm.) (*E*) Bacterial burdens as assessed by bacterial fluorescence. Statistics: One-way ANOVA with Dunnett's test. (*F*) Average infection foci size per larva. Statistics: One-way ANOVA with Dunnett's test. Data are representative of three independent experiments. Statistics: ****$P < 0.0001$, ***$P \leq 0.001$; not significant (ns), $P > 0.05$.

membrane damage. In turn, this level of phagosomal damage was sufficient for relatively high levels of in vivo growth compared to ESX-1–deficient Mm. Our findings led us to revisit our previous conclusions that an Mm ESAT-6 M93T C-terminal point mutant lost phagosomal membrane damage and early virulence solely due to reduced secretion (8). The Mm–ESAT-6 M93T mutant allowed for much greater levels of ESAT-6 secretion than the Mm-*eccA1*::Tn mutant, showing that C-terminal integrity was needed for ESAT-6's direct membrane damaging and virulence effects. We solidified this conclusion through experiments demonstrating that the Mm–ESAT-6 M83I mutant had a similar dissociation between secretion and virulence phenotypes. In the course of this analysis, we found that in vivo ESAT-6–mediated phagosomal lysis by Mtb and Mm was enhanced in acidic compartments. This suggested that the pH-dependent lytic activity of purified ESAT-6 was a direct correlate of phagosomal damage. However, we found that purified ESAT-6 M93T retained full activity in lysing acidified liposomes.

Previous studies examining both transposon mutants and total knockouts of *eccA1* have found defects in hemolysis and in vivo growth similar to those we observed in Mm-*eccA1*::Tn (7, 36). A genome-wide Mtb transposon mutant screen in both cultured macrophages and the mouse TB model identified *eccA1*::Tn mutants as being attenuated (54–56). These findings are broadly consistent with ours, although in the absence of direct comparisons, it is not clear whether EccA1 is less important than the full ESX-1 locus in Mtb infection as well. Our findings that minimal ESAT-6 secretion is compatible with

substantial preservation of early Mm infection phenotypes are also in line with prior observations of phagosomal damage (as reflected by cytosolic translocation of mycobacteria) in ESAT-6 secretion–deficient Mm mutants (31). We see two possible explanations for this. First, minute amounts of secretion that are not detected by immunoblotting could be sufficient for ESX-1 function (32, 57). Second, surface-bound ESAT-6 can partially compensate for the lack of secretion during early infection. Two studies have found that the retention of surface-bound ESAT-6 correlates with pathogenic phenotypes (35, 37). Furthermore, an earlier report on Δ*eccA1* found wild-type levels of ESAT-6 in bacterial cell surface extracts despite an overall reduction in ESX-1 secretion (36).

ESAT-6 binds to CFP-10 to form a heterodimeric complex and the two proteins are likely cosecreted (58). ESAT-6's C terminus does not participate in binding to CFP-10 (Fig. 2*A*) and truncation of this region (Δ84 to 95) does not affect secretion, likely as the CFP-10's C-terminal tail is responsible for recognition and secretion of the heterodimer (58–61). However, conservation of ESAT-6's C terminus among mycobacterial homologs (*SI Appendix*, Fig. S3) suggests it mediates an essential function beyond secretion. Consistent with this, an Mtb mutant expressing the C-terminal ESAT-6 truncation has reduced phagosomal permeabilization as reflected by translocation into the cytosol (59). Furthermore, it was reported that complementation of *Mycobacterium bovis* bacillus Calmette–Guérin with an ESX-1 cosmid expressing truncated ESAT-6 did not rescue attenuation (45). This region appears to be highly conserved in clinical strains: We
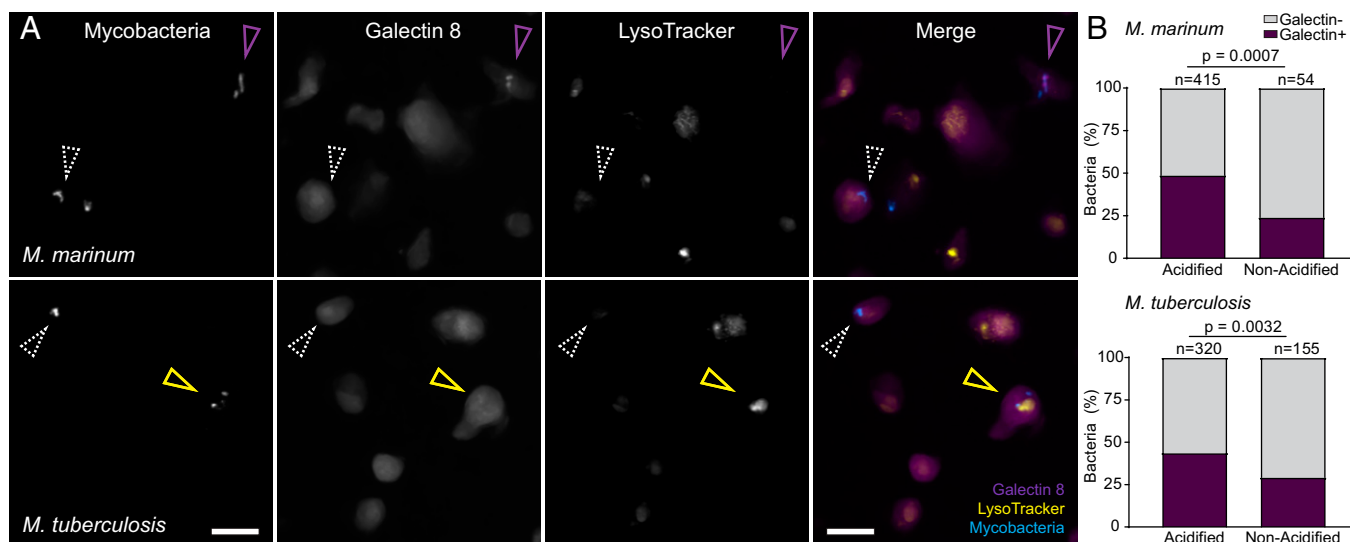
Osman et al.
The C terminus of the mycobacterium ESX-1 secretion system substrate ESAT-6 is required for phagosomal membrane damage and virulence

PNAS | 5 of 9
https://doi.org/10.1073/pnas.2122161119

Fig. 5. Mm- and Mtb-mediated phagosomal membrane damage is enhanced in acidified phagosomes. (*A* and *B*) Galectin-8 labeled, LysoTracker Red-stained THP-1 cells at 24 h postinfection with EBFP2-expressing Mm (*Top*) or Mtb (*Bottom*). (*A*) Representative images of mycobacteria, Galectin-8, or LysoTracker, shown individually or as a merge of all three channels. (Scale bar, 10 μm.) Magenta arrowhead, bacteria proximal to galectin-8 puncta. Yellow arrowhead, acidified bacteria proximal to galectin-8 puncta. White arrowhead, bacteria that did not induce galectin-8 puncta. (*B*) Percent of bacteria located proximal to galectin-8 puncta, sorted by colocalization with LysoTracker positive compartments. Statistics: Fisher's exact test.

examined the genome-wide *Mycobacterium tuberculosis* variation database of 2,819 Mtb isolates for occurrences of nonsynonymous (coding) mutations in *esxA* and of the eight occurrences of nonsynonymous mutations in *esxA*; none were in located in the conserved C-terminal motif (residues 83 to 95) (62).

Our finding that phagosomal acidification greatly enhances ESAT-6–mediated damage supports the model that ESAT-6's pH-dependent functions in vitro are physiologically relevant (16, 21, 40). This assay does not fully capture ESAT-6's in vivo role, as mycobacteria in nonacidified compartments still induced phagosomal damage to a greater extent than either of

Fig. 6. Recombinant ESAT-6–M93T has wild-type levels of acidified liposome lysis activity. Quantification of pH-dependent liposome lysis by 3 μM recombinant ESAT-6 as measured by fluorescent ANTS release from DOPC liposomes. Statistics: One-way ANOVA with Šidák's multiple comparisons test, ****$P < 0.0001$; not significant (ns), $P > 0.05$. Data are combined from four experimental replicates.

the C-terminal ESAT-6 mutants. However, it is likely that ESAT-6's activity under acidic pH mimics an aspect of its in vivo function. This is further supported by the recent finding that membrane vesicles prepared using lipids from the THP-1 human monocytic cell line are also damaged by ESAT-6 (recombinant and native) only at acidic pH (23, 26). On this backdrop, it is interesting to consider the role of the ESAT-6 C terminus in phagosomal damage, particularly of the two point mutants examined here. It has been shown that in the context of acidified liposome lysis, the ESAT-6 C terminus does not insert into the membrane and remains solvent-exposed (46). NMR and crystal structures of the heterodimer predict that the tail is floppy and unstructured (44, 58). However, the authors who solved the crystal structure suggested that this region could also adopt an alpha-helical structure in vivo (44). This was based on identification of a C-terminal motif conserved across actinobacterial ESAT-6 homologs that is consistent with an alpha-helical structure (44). This hypothesis is supported by the recent AlphaFold2 structural prediction of ESAT-6 with a structured C terminus (63) (Fig. 2*C*). This disparity between experimental and predicted structure could reflect a conformational versatility of the C terminus that is required for different aspects of ESAT-6's in vivo functions.

The ESAT-6 C-terminal tail resides on the exterior of lipid membranes following insertion (46). While an ESAT-6 C-terminal truncation mutant can insert into liposome membranes, it has reduced lytic activity (46). This suggests a direct role for the C terminus in enabling "basal" ESAT-6 membranolytic function. The ESAT-6 M93T and M83I point mutants are relatively conservative. As methionine and isoleucine are both small hydrophobic residues, an isoleucine mutation is highly conservative, while threonine, as a small polar residue would be less so. Neither of these mutations would be predicted to be particularly disruptive to C-terminal structure, and in this light, perhaps it is not surprising after all that the M93T mutation does not affect its in vitro basal membranolytic activity. Rather, this finding suggests that the M93T mutant is defective in a C-terminally mediated function that is required for robust in vivo lysis. Following membrane insertion, the C terminus could enhance oligomerization of ESAT-6, interactions with mycobacterial or host factors, or act as a bacterial sensor for
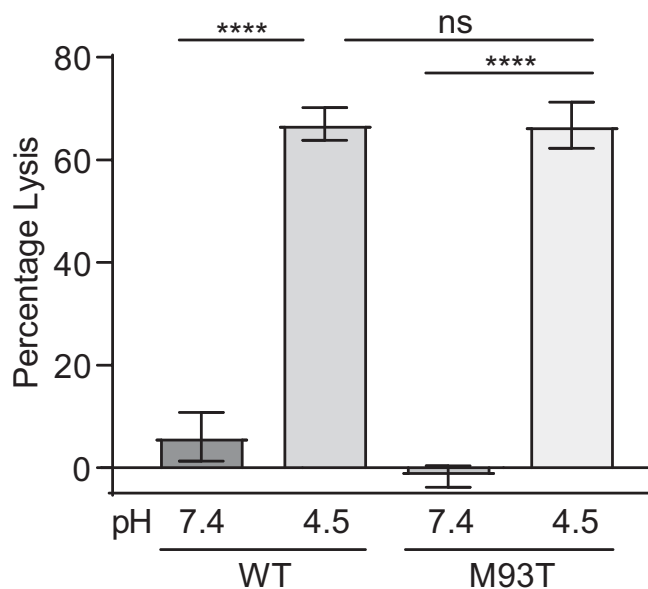
contact-dependent lysis by ESX-1, or any combination of these. Putative mycobacterial factors include other ESX-1 substrates that contribute to virulence in addition to ESAT-6, such as EspA, EspE, or EspF (9, 32, 64), or oligomers of EspB and EspC, which are proposed to be part of a putative extracellular secretory complex mediating contact-dependent lysis (65, 66). A systematic mutational analysis of the C terminus coupled with biochemical studies to identify mycobacterial, or possibly even host, determinants that bind to wild type but not M93T and other in vivo deficient ESAT-6 mutants may pave the way to a fuller understanding of ESAT-6's in vivo function.

Materials and Methods

Bacterial Strains and Culture Methods. All Mm and Mtb strains used are listed in *SI Appendix*, Table S3. Mm strains were all derived from wild-type Mm purchased from American Type Culture Collection (strain M, ATCC #BAA-535). Mm strains were grown without agitation at 33 °C in 7H9 Middlebrook's medium (Difco) supplemented with 10% oleic acid albumin dextrose saline (OADS) and 0.05% Tween-80 (Sigma) with appropriate selection (50 µg/mL hygromycin [Mediatech] and 20 µg/mL kanamycin [Sigma]) or on supplemented Middlebrook 7H10 agar (Millipore) (no Tween-80) (67). Mtb mc^{2}6206 strains (51) were grown without agitation at 37 °C in 7H9 Middlebrook's medium (Difco) supplemented with 10% Middlebrook oleic acid albumin dextrose catalase (OADC) supplement (Becton Dickinson), 0.05% Tween-80 (Sigma), 12 µg/mL pantothenic acid (Sigma), and 25 µg/mL L-leucine (Sigma) with appropriate selection (20 µg/mL kanamycin [Sigma]) or on supplemented Middlebrook 7H10 agar (Millipore) (no Tween-80).

Generation of Mutant Strains. The *eccA1*::Tn mutant was isolated from a Mm transposon mutant library. Briefly, a novel *mariner*-based mini transposon containing an excisable hygromycin-resistance cassette was used to mutagenize wild-type Mm in small batches and individual colonies were isolated and sequenced. The transposon insertion in *eccA1*::Tn was confirmed by semirandom, nested PCR and located 16.26% into the *eccA1* open reading frame, as measured by distance from the ATG start site.

The Mm-Δ*esxA* mutant was generated using phage transduction (68). Briefly, a fragment containing sequences flanking *esxA* (23 to 955 bp upstream of the ATG, 13 to 1,101 bp downstream of its stop codon) were cloned into pYUB854 to generate pYUB854-*esxA*. The resulting cosmid was digested with *PacI* (NEB) and the insert was ligated into phAE159 (a gift from William Jacobs, Albert Einstein College of Medicine, New York, NY) to generate the phSP105 phasmid. Following ligation, packaging, and transduction, phSP105 was transformed into *Mycobacterium smegmatis* mc^{2}155. Harvested phages were transduced into wild-type Mm and plated on 7H10-Hyg. Positive colonies were confirmed by Southern blotting, and the hygromycin cassette was excised by transformation with pYUB870. Loss of pYUB870 was confirmed by plating on 7H10 + sucrose plates, and excision of cassette was confirmed via PCR.

Complementation Constructs. Mm-Δ*esxA* was complemented with pMH406 (69). ESAT-6-M83I and ESAT-6-M93T complementation constructs (*SI Appendix*, Table S1) were generated via site-directed mutagenesis using primers listed in *SI Appendix*, Table S2.

Single-Cell Suspensions of Mycobacteria. Single-cell suspensions of mycobacteria were prepared as previously described (67) with minor modifications. Briefly, mycobacteria were cultured with antibiotic selection to midlog (optical density [OD]$_{600}$ = 0.3 to 0.6) and then pelleted at 3,220 × *g* for 20 min at 20 °C. The top layer of the pellet containing precipitated kanamycin was discarded following gentle scraping with a disposable inoculating loop. The underlying pellet was resuspended in 5 mL 7H9 media supplemented with 10% OADS (no Tween-80) and then passed 10 times through a 27-gauge blunt needle. Mycobacteria were then pelleted at 100 × *g* for 1 min. A total of 4 mL supernatant was collected. The bacterial pellet was resuspended in 5 mL of 7H9 OADS. Mycobacteria were again passed 10 times through a blunt needle, pelleted at 100 × *g*, and supernatant was collected. This was repeated until 15 mL of supernatant was collected. The supernatant was then passed through a 5-µm syringe filter (Pall, 4650) to isolate single-cell bacteria. Single-cell bacteria were concentrated by centrifugation at 3,220 × *g* for 30 min at room temperature. The pellet was then resuspended in 200 µL 7H9 OADS, divided into 5-µL aliquots, and stored at −80 °C. Mycobacterial concentration was determined by plating for colony-forming units (CFU).

Intramacrophage Growth Assays. Growth assays were performed as described previously with minor modifications (8). J774A.1 cells were maintained in Gibco's Dulbecco's modified Eagle medium (DMEM). Twenty-four hours before infection, cells were scraped and resuspended in DMEM to a concentration of 2.5×10^5 cells/mL. J774A.1 cells were plated in a 24-well optical bottom tissue culture plate (Perkin-Elmer, 1450-606) by aliquoting 500 µL of this cell suspension to each well and then incubating at 37 °C overnight. The following day, cells were washed twice with phosphate-buffered saline (PBS) and infected with antibiotic-free media containing single-cell suspensions of tdTomato-expressing Mm at a multiplicity of infection of ~0.25 (wild-type, *eccA1*::Tn,::*esxA*) or ~0.5 (attenuated strains) for 4 h at 33 °C, 5% CO$_2$. After infection, cells were washed twice with PBS, 500 µL fresh media added to each well, and then incubated at 33 °C, 5% CO$_2$. Cells were imaged by fluorescence microscopy at indicated timepoints using a Nikon Eclipse Ti-E equipped with a Ti-S-E Motor XY Stage, a C-HGFIE 130-W mercury light source, a 23/0.10 Plan Apochromat objective, and a Chroma ET-CY3 (49004) filter cube. Fluorescence images were captured with a Photometrics CoolSNAP HQ2 monochrome camera, using NIS-Elements (version 3.22). Resulting images were analyzed in ImageJ using a custom script for fluorescence pixel count (FPC) to determine bacterial burden (67).

Galectin-8 Immunofluorescence. THP-1 cells were diluted to 5×10^5 cells/mL in RPMI + 10% fetal bovine serum (Gibco) and treated with 100 nM phorbol 12-myristate-13-acetate (PMA) (Sigma, P1585). THP-1 cells were plated in a 24-well optical bottom tissue culture plate (Perkin-Elmer, 1450-606) by aliquoting 500 µL of this cell suspension to each well and then incubating at 37 °C for 2 d. PMA-containing media were then removed and replaced with fresh media, and the cells were allowed to rest for a day. The following day, cells were washed twice with PBS and infected with antibiotic-free media containing single-cell suspensions of tdTomato-expressing Mm at a multiplicity of infection of ~1 for 4 h at 33 °C, 5% CO$_2$. After infection, cells were washed twice with PBS, 500 µL fresh media added to each well, and then incubated overnight at 33 °C, 5% CO$_2$.

Galectin-8 staining was done as previously described (28). Briefly, 24 h after infection, cells were fixed in 4% (wt/vol) paraformaldehyde in PBS at room temperature for at least 30 min. Fixed cells were washed twice with PBS and then incubated in permeabilization/block (PB) buffer for 30 min at room temperature and then stained with goat anti-human galectin-8 antibody (R&D Systems, AF1305) diluted in PB solution overnight at 4 °C. Cells were then washed three times with PBS and stained with AlexaFluor 488-conjugated donkey anti-goat IgG (Thermo Fisher, A-11055) diluted in PB solution for 1 h at room temperature. Cells were then washed three times in PBS and imaged.

LysoTracker experiments were conducted as above with the following modifications: Cells were infected with EBFP2-expressing Mm or Mtb at an MOI of ~0.5. The next day, cells were stained with 100 nM of LysoTracker Red DND-99 (Invitrogen) in RPMI for 45 min at 33 °C and then immediately fixed and stained as above. Acidic organelles, fluorescent bacteria, and galectin-8 puncta were identified using the three-dimensional (3D) surface rendering feature of Imaris (Bitplane Scientific Software). Bacteria were scored as galectin-8 positive if they were located within 2 µm of a galectin-8 surface and as acidified if they were located within a LysoTracker surface.

Zebrafish Husbandry. All zebrafish husbandry and experiments were performed in compliance with the UK Home Office and the Animal Ethics Committee of the University of Cambridge.

Zebrafish maintenance and spawning were performed as previously described (67). Briefly, zebrafish were maintained on a recirculating aquaculture system with a 14-h light/10-h dark cycle. Fish were fed dry food and brine shrimp twice a day. Adult wild-type AB line zebrafish were spawned and embryos collected and then housed in fish water (reverse osmosis water containing 0.18 g/L Instant Ocean) at 28.5 °C. The fish water was supplemented with 0.25 µg/mL methylene blue from collection to 1 d postfertilization (dpf), and at 1 dpf, 0.003% 1-phenyl-2-thiourea (PTU) (Sigma) was added to prevent pigmentation.

Zebrafish Infections. Zebrafish larvae were infected with the indicated strains of tdTomato-expressing Mm by injection into the caudal vein at 2 dpf using freshly thawed single-cell suspensions diluted to the same CFU/µL. Injection dose was plated on 7H10 + 10% OADS with appropriate antibiotic to ensure a similar infection dose.

Measuring Bacterial Burden in Larvae. Fluorescence microscopy was performed as previously described (67). Briefly, infected larvae were imaged by fluorescence microscopy at 5 dpf using a Nikon Eclipse Ti-E equipped with a Ti-S-E Motor XY Stage, a C-HGFIE 130-W mercury light source, a 23/0.10 Plan Apochromat objective, and a Chroma ET-CY3 (49004) filter cube. Fluorescence

Osman et al.
The C terminus of the mycobacterium ESX-1 secretion system substrate ESAT-6 is required for phagosomal membrane damage and virulence

PNAS | 7 of 9
https://doi.org/10.1073/pnas.2122161119

images were captured with a Photometrics CoolSNAP HQ2 monochrome camera, using NIS-Elements (version 3.22). The resulting images were analyzed in ImageJ using a custom script for FPC to determine bacterial burden and infection foci size.

Secretion Assay. Culture filtrate (CF) fractions and cell pellet (CP) fractions were prepared as described previously (8). Mm was grown to mid-to-late log stage, washed with PBS, resuspended to a final OD_{600} of 0.8 to 1.0 in 50 mL of modified Sauton's media, and incubated for 48 h at 33 °C. A total of 10 μg of CP and 20 μg of CF were loaded per well for sodium dodecyl sulfate–polyacrylamide gel electrophoresis (SDS-PAGE), and presence of ESAT-6, CFP-10, and GroEL2 was determined by Western blotting with mouse anti–ESAT-6 clone 11G4 (1:3,000; Thermo Fisher, HYB-076-08-02), rabbit anti-CFP-10 (1:5,000; BEI, product NR13801), or mouse anti-GroEL2 clone IT-56 (1:1,000; BEI, product NR-13655) primary antibody followed by horseradish peroxidase–conjugated goat anti-mouse (1:10,000; Stratech 115-035-003-JIR) (Fig. 3*B* and *SI Appendix*, Fig. S2), goat anti-mouse IgG DyLight 800 (1:15,000 Cell Signaling Technology #5257S), or goat anti-rabbit IgG DyLight 800 (1:15,000 Cell Signaling Technology #5151S) secondary antibody. Chemiluminescence detection was then performed using Amersham ECL Western Blotting Detection Reagents (GE Lifesciences) and fluorescence imaging performed on a LI-COR Odyssey.

Hemolysis Assay. Hemolytic activity was assessed as described previously (8). Briefly, 100 μL of 1% (vol/vol) sheep RBCs (Fisher Scientific) in PBS was combined with 100 μL of PBS, bacterial suspension, or 0.1% Triton X-100 (Sigma), pelleted, and then incubated for 2 h at 33 °C. Pellets were resuspended, repelleted, and the absorbance of the supernatant was measured at 405 nm. Raw absorbance data were converted to percentage lysis, by subtracting PBS lysis (background lysis) and dividing by 0.1% Triton X-100 lysis (complete lysis).

Protein Expression and Purification. Expression of recombinant ESAT-6 was conducted as previously done (8) with the following modifications: Bacterial pellets were resuspended in 5 mL of lysis buffer (150 mM NaCl, 20 mM Tris pH 8, 5 mM imidazole) per gram of pellet and then sonicated on ice. Lysates were clarified by centrifugation at 15,000 × g for 30 min at 4 °C. Clarified lysate was added to 1 mL of washed nickel-nitrilotriacetic acid bead slurry (Qiagen) and incubated for 1 h at 4 °C. Beads were then pelleted and washed with 10 column volumes (CVs) of lysis buffer. Next, beads were washed with 10 CVs of binding buffer (150 mM NaCl, 20 mM Tris pH 8, 20 mM imidazole), followed by 15 CVs of wash buffer (150 mM NaCl, 20 mM Tris pH 8, 75 mM imidazole). Three CVs of elution buffer (150 mM NaCl, 20 mM Tris pH 8, 1 M imidazole) were added to the elute protein. Eluate was concentrated and then loaded on a S75 size exclusion column (GE Healthcare) equilibrated with 150 mM NaCl, 20 mM Tris, pH 8. Fractions were collected and monitored for recombinant

protein elution and purity by SDS-PAGE followed by Coomassie staining. Protein concentration from highly purified eluted fractions was quantified by absorbance at 280 nm. Constructs for mutant protein purification (*SI Appendix*, Table S1) were generated via site-directed mutagenesis using primers listed in *SI Appendix*, Table S2.

Liposome Lysis Assay. Liposomes containing ANTS were generated as previously described with modifications (8). Briefly, 1,2-dioleoyl-sn-glycero-3-phosphocholine (Sigma) was dissolved in 86 μL of chloroform (Sigma) to 100 mg/mL. The resulting solution was transferred to a glass vial and chloroform was evaporated under N_2 gas and subsequently under vacuum overnight. Lipid films were resuspended in 400 μL of 125 mM ANTS (Invitrogen) in PBS by vortexing. Liposomes were generated by five freeze–thaw cycles by freezing in liquid nitrogen for 3 min and then thawing in a 40 to 50 °C water bath for 3 min. Liposomes were then extruded 25 times through two 200-nm polycarbonate Nucleopore filters (Whatman) and then washed in PBS by centrifugation at 60,000 × g for 30 min at 4 °C. Liposomes were resuspended in 400 μL PBS for use in assays.

Stock solutions of 200 mM sodium phosphate and 100 mM citric acid with 150 mM NaCl were used to generate pH 4.5 and 7.4 phosphate-citrate pH buffers (pH buffer). The pH value of each buffer was confirmed after preparation. To measure liposome lytic activity of recombinant proteins, 5 μL of liposomes was resuspended in 200 μL pH buffer and 3 μM rESAT-6 or an equivalent volume of vehicle was added. Protein and liposome samples were incubated with rotation at 20 °C for 30 min in ultracentrifuge tubes. Intact liposomes were pelleted by centrifugation at 1,800,000 × g for 30 min at 4 °C and then ANTS fluorescence in the supernatants was measured (excitation/emission [nm]: 350 ± 15/520 ± 15). Raw fluorescence data were converted to percentage of lysis by subtracting buffer only lysis (background lysis) and dividing by 0.05% Triton X-100 lysis (complete lysis) at each pH.

Data Availability. All study data are included in the article and/or *SI Appendix*.

1. K. N. Lewis *et al.*, Deletion of RD1 from *Mycobacterium tuberculosis* mimics bacille Calmette-Guérin attenuation. *J. Infect. Dis.* **187**, 117–123 (2003).
2. A. S. Pym, P. Brodin, R. Brosch, M. Huerre, S. T. Cole, Loss of RD1 contributed to the attenuation of the live tuberculosis vaccines *Mycobacterium bovis* BCG and *Mycobacterium microti*. *Mol. Microbiol.* **46**, 709–717 (2002).
3. H. E. Volkman *et al.*, Tuberculous granuloma formation is enhanced by a mycobacterium virulence determinant. *PLoS Biol.* **2**, e367 (2004).
4. P. Brodin, I. Rosenkrands, P. Andersen, S. T. Cole, R. Brosch, ESAT-6 proteins: Protective antigens and virulence factors? *Trends Microbiol.* **12**, 500–508 (2004).
5. G. G. Mahairas, P. J. Sabo, M. J. Hickey, D. C. Singh, C. K. Stover, Molecular analysis of genetic differences between *Mycobacterium bovis* BCG and virulent *M. bovis*. *J. Bacteriol.* **178**, 1274–1282 (1996).
6. W. Bitter *et al.*, Systematic genetic nomenclature for type VII secretion systems. *PLoS Pathog.* **5**, e1000507 (2009).
7. L. Y. Gao *et al.*, A mycobacterial virulence gene cluster extending RD1 is required for cytolysis, bacterial spreading and ESAT-6 secretion. *Mol. Microbiol.* **53**, 1677–1693 (2004).
8. W. H. Conrad *et al.*, Mycobacterial ESX-1 secretion system mediates host cell lysis through bacterium contact-dependent gross membrane disruptions. *Proc. Natl. Acad. Sci. U.S.A.* **114**, 1371–1376 (2017).
9. A. E. Chirakos, A. Balaram, W. Conrad, P. A. Champion, Modeling tubercular ESX-1 secretion using *Mycobacterium marinum*. *Microbiol. Mol. Biol. Rev.* **84**, e00082-19 (2020).
10. C. J. Cambier, S. Falkow, L. Ramakrishnan, Host evasion and exploitation schemes of *Mycobacterium tuberculosis*. *Cell* **159**, 1497–1509 (2014).
11. H. E. Volkman *et al.*, Tuberculous granuloma induction via interaction of a bacterial secreted protein with host epithelium. *Science* **327**, 466–469 (2010).
12. J. M. Davis, L. Ramakrishnan, The role of the granuloma in expansion and dissemination of early tuberculous infection. *Cell* **136**, 37–49 (2009).
13. R. Simeone, L. Majlessi, J. Enninga, R. Brosch, Perspectives on mycobacterial vacuole-to-cytosol translocation: The importance of cytosolic access. *Cell. Microbiol.* **18**, 1070–1077 (2016).
14. N. van der Wel *et al.*, *M. tuberculosis* and *M. leprae* translocate from the phagolysosome to the cytosol in myeloid cells. *Cell* **129**, 1287–1298 (2007).
15. J. Smith *et al.*, Evidence for pore formation in host cell membranes by ESX-1-secreted ESAT-6 and its role in *Mycobacterium marinum* escape from the vacuole. *Infect. Immun.* **76**, 5478–5487 (2008).
16. Y. Bao, L. Wang, J. Sun, A small protein but with diverse roles: A review of EsxA in mycobacterium-host interaction. *Cells* **10**, 1675 (2021).
17. A. L. Sørensen, S. Nagai, G. Houen, P. Andersen, A. B. Andersen, Purification and characterization of a low-molecular-mass T-cell antigen secreted by *Mycobacterium tuberculosis*. *Infect. Immun.* **63**, 1710–1717 (1995).
18. M. J. Pallen, The ESAT-6/WXG100 superfamily – And a new Gram-positive secretion system? *Trends Microbiol.* **10**, 209–212 (2002).
19. M. M. Champion, E. A. Williams, R. S. Pinapati, P. A. Champion, Correlation of phenotypic profiles using targeted proteomics identifies mycobacterial esx-1 substrates. *J. Proteome Res.* **13**, 5151–5164 (2014).
20. S. M. Fortune *et al.*, Mutually dependent secretion of proteins required for mycobacterial virulence. *Proc. Natl. Acad. Sci. U.S.A.* **102**, 10676–10681 (2005).
21. M. I. de Jonge *et al.*, ESAT-6 from *Mycobacterium tuberculosis* dissociates from its putative chaperone CFP-10 under acidic conditions and exhibits membrane-lysing activity. *J. Bacteriol.* **189**, 6028–6034 (2007).
22. T. Hsu *et al.*, The primary mechanism of attenuation of bacillus Calmette-Guerin is a loss of secreted lytic function required for invasion of lung interstitial tissue. *Proc. Natl. Acad. Sci. U.S.A.* **100**, 12420–12425 (2003).
23. J. Augenstreich *et al.*, Phthiocerol dimycocerosates from *Mycobacterium tuberculosis* increase the membrane activity of bacterial effectors and host receptors. *Front. Cell. Infect. Microbiol.* **10**, 420 (2020).
24. Y. Bao *et al.*, Mycobacterial surface-associated ESX-1 virulence factors play a role in mycobacterial adherence and invasion into lung epithelial cells. bioRxiv [Preprint] (2020). https://www.biorxiv.org/content/10.1101/2020.10.13.337667v1.full. Accessed 8 December 2021.
25. A. K. Barczak *et al.*, Systematic, multiparametric analysis of *Mycobacterium tuberculosis* intracellular infection offers insight into coordinated virulence. *PLoS Pathog.* **13**, e1006363 (2017).

8 of 9 | PNAS
https://doi.org/10.1073/pnas.2122161119

Osman et al.
The C terminus of the mycobacterium ESX-1 secretion system substrate ESAT-6 is required for phagosomal membrane damage and virulence

26. J. Augenstreich et al., ESX-1 and phthiocerol dimycocerosates of *Mycobacterium tuberculosis* act in concert to cause phagosomal rupture and host cell apoptosis. *Cell. Microbiol.* **19**, e12726 (2017).

27. J. Quigley et al., The cell wall lipid PDIM contributes to phagosomal escape and host cell exit of *Mycobacterium tuberculosis*. *mBio* **8**, e00148-17 (2017).

28. M. M. Osman, A. J. Pagán, J. K. Shanahan, L. Ramakrishnan, *Mycobacterium marinum* phthiocerol dimycocerosates enhance macrophage phagosomal permeabilization and membrane damage. *PLoS One* **15**, e0233252 (2020).

29. T. R. Lerner et al., Phthiocerol dimycocerosates promote access to the cytosol and intracellular burden of *Mycobacterium tuberculosis* in lymphatic endothelial cells. *BMC Biol.* **16**, 1 (2018).

30. A. E. Chirakos, K. R. Nicholson, A. Huffman, P. A. Champion, Conserved ESX-1 substrates EspE and EspF are virulence factors that regulate gene expression. *Infect. Immun.* **88**, e00289-20 (2020).

31. J. Lienard et al., The *Mycobacterium marinum* ESX-1 system mediates phagosomal permeabilization and type I interferon production via separable mechanisms. *Proc. Natl. Acad. Sci. U.S.A.* **117**, 1160–1166 (2020).

32. J. M. Chen et al., Phenotypic profiling of *Mycobacterium tuberculosis* EspA point mutants reveals that blockage of ESAT-6 and CFP-10 secretion in vitro does not always correlate with attenuation of virulence. *J. Bacteriol.* **195**, 5421–5430 (2013).

33. S. A. Joshi et al., EccA1, a component of the *Mycobacterium marinum* ESX-1 protein virulence factor secretion pathway, regulates mycolic acid lipid synthesis. *Chem. Biol.* **19**, 372–380 (2012).

34. R. E. Bosserman, K. R. Nicholson, M. M. Champion, P. A. Champion, A new ESX-1 substrate in *Mycobacterium marinum* that is required for hemolysis but not host cell lysis. *J. Bacteriol.* **201**, e00760-18 (2019).

35. G. M. Kennedy, G. C. Hooley, M. M. Champion, F. Mba Medie, P. A. Champion, A novel ESX-1 locus reveals that surface-associated ESX-1 substrates mediate virulence in *Mycobacterium marinum*. *J. Bacteriol.* **196**, 1877–1888 (2014).

36. T. H. Phan et al., EspH is a hypervirulence factor for *Mycobacterium marinum* and essential for the secretion of the ESX-1 substrates EspE and EspF. *PLoS Pathog.* **14**, e1007247 (2018).

37. J. Raffetseder, N. Iakobachvili, V. Loitto, P. J. Peters, M. Lerm, Retention of EsxA in the capsule-like layer of *Mycobacterium tuberculosis* is associated with cytotoxicity and is counteracted by lung surfactant. *Infect. Immun.* **87**, e00803-18 (2019).

38. Q. Zhang et al., EsxA membrane-permeabilizing activity plays a key role in mycobacterial cytosolic translocation and virulence: Effects of single-residue mutations at glutamine 5. *Sci. Rep.* **6**, 32618 (2016).

39. Y. Bao, L. Wang, J. Sun, Post-translational knockdown and post-secretional modification of EsxA determine contribution of EsxA membrane permeabilizing activity for mycobacterial intracellular survival. *Virulence* **12**, 312–328 (2021).

40. J. De Leon et al., *Mycobacterium tuberculosis* ESAT-6 exhibits a unique membrane-interacting activity that is not found in its ortholog from non-pathogenic *Mycobacterium smegmatis*. *J. Biol. Chem.* **287**, 44184–44191 (2012).

41. J. Jia et al., Galectins control mTOR in response to endomembrane damage. *Mol. Cell* **70**, 120–135.e8 (2018).

42. K. B. Boyle, F. Randow, The role of 'eat-me' signals and autophagy cargo receptors in innate immunity. *Curr. Opin. Microbiol.* **16**, 339–348 (2013).

43. M. M. Osman et al., Ebselen attenuates mycobacterial virulence through inhibition of ESX-1 secretion. bioRxiv [Preprint] (2021). https://www.biorxiv.org/content/10.1101/828574v2. Accessed 14 December 2021.

44. C. Poulsen, S. Panjikar, S. J. Holton, M. Wilmanns, Y. H. Song, WXG100 protein superfamily consists of three subfamilies and exhibits an α-helical C-terminal conserved residue pattern. *PLoS One* **9**, e89313 (2014).

45. P. Brodin et al., Functional analysis of early secreted antigenic target-6, the dominant T-cell antigen of *Mycobacterium tuberculosis*, reveals key residues involved in secretion, complex formation, virulence, and immunogenicity. *J. Biol. Chem.* **280**, 33953–33959 (2005).

46. Y. Ma, V. Keil, J. Sun, Characterization of *Mycobacterium tuberculosis* EsxA membrane insertion: Roles of N- and C-terminal flexible arms and central helix-turn-helix motif. *J. Biol. Chem.* **290**, 7314–7322 (2015).

47. R. Simeone et al., Cytosolic access of *Mycobacterium tuberculosis*: Critical impact of phagosomal acidification control and demonstration of occurrence in vivo. *PLoS Pathog.* **11**, e1004650 (2015).

48. S. van der Niet et al., IL-1R1-dependent signals improve control of cytosolic virulent mycobacteria in vivo. *mSphere* **6**, e00153-21 (2021).

49. J. F. Dermine et al., Flotillin-1-enriched lipid raft domains accumulate on maturing phagosomes. *J. Biol. Chem.* **276**, 18507–18512 (2001).

50. S. Levitte et al., Mycobacterial acid tolerance enables phagolysosomal survival and establishment of tuberculous infection in vivo. *Cell Host Microbe* **20**, 250–258 (2016).

51. C. Vilchèze et al., Rational design of biosafety level 2-approved, multidrug-resistant strains of *Mycobacterium tuberculosis* through nutrient auxotrophy. *mBio* **9**, e00938-18 (2018).

52. K. S. Beckwith et al., Plasma membrane damage causes NLRP3 activation and pyroptosis during *Mycobacterium tuberculosis* infection. *Nat. Commun.* **11**, 2270 (2020).

53. X. Peng, J. Sun, Mechanism of ESAT-6 membrane interaction and its roles in pathogenesis of *Mycobacterium tuberculosis*. *Toxicon* **116**, 29–34 (2016).

54. J. Rengarajan, B. R. Bloom, E. J. Rubin, Genome-wide requirements for *Mycobacterium tuberculosis* adaptation and survival in macrophages. *Proc. Natl. Acad. Sci. U.S.A.* **102**, 8327–8332 (2005).

55. C. M. Sassetti, E. J. Rubin, Genetic requirements for mycobacterial survival during infection. *Proc. Natl. Acad. Sci. U.S.A.* **100**, 12989–12994 (2003).

56. Y. J. Zhang et al., Tryptophan biosynthesis protects mycobacteria from CD4 T-cell-mediated killing. *Cell* **155**, 1296–1308 (2013).

57. P. A. Champion, Disconnecting in vitro ESX-1 secretion from mycobacterial virulence. *J. Bacteriol.* **195**, 5418–5420 (2013).

58. P. S. Renshaw et al., Structure and function of the complex formed by the tuberculosis virulence factors CFP-10 and ESAT-6. *EMBO J.* **24**, 2491–2498 (2005).

59. D. Houben et al., ESX-1-mediated translocation to the cytosol controls virulence of mycobacteria. *Cell. Microbiol.* **14**, 1287–1298 (2012).

60. O. S. Rosenberg et al., Substrates control multimerization and activation of the multi-domain ATPase motor of type VII secretion. *Cell* **161**, 501–512 (2015).

61. P. A. Champion, S. A. Stanley, M. M. Champion, E. J. Brown, J. S. Cox, C-terminal signal sequence promotes virulence factor secretion in *Mycobacterium tuberculosis*. *Science* **313**, 1632–1636 (2006).

62. E. N. Chernyaeva et al., Genome-wide *Mycobacterium tuberculosis* variation (GMTV) database: A new tool for integrating sequence variations and epidemiology. *BMC Genomics* **15**, 308 (2014).

63. J. Jumper et al., Highly accurate protein structure prediction with AlphaFold. *Nature* **596**, 583–589 (2021).

64. D. Bottai et al., ESAT-6 secretion-independent impact of ESX-1 genes espF and espG1 on virulence of *Mycobacterium tuberculosis*. *J. Infect. Dis.* **203**, 1155–1164 (2011).

65. Y. Lou, J. Rybniker, C. Sala, S. T. Cole, EspC forms a filamentous structure in the cell envelope of *Mycobacterium tuberculosis* and impacts ESX-1 secretion. *Mol. Microbiol.* **103**, 26–38 (2017).

66. A. Gijsbers et al., Priming mycobacterial ESX-secreted protein B to form a channel-like structure. *Curr. Res. Struct. Biol.* **3**, 153–164 (2021).

67. K. Takaki, J. M. Davis, K. Winglee, L. Ramakrishnan, Evaluation of the pathogenesis and treatment of *Mycobacterium marinum* infection in zebrafish. *Nat. Protoc.* **8**, 1114–1124 (2013).

68. S. Bardarov et al., Specialized transduction: An efficient method for generating marked and unmarked targeted gene disruptions in *Mycobacterium tuberculosis*, *M. bovis* BCG and *M. smegmatis*. *Microbiology (Reading)* **148**, 3007–3017 (2002).

69. K. M. Guinn et al., Individual RD1-region genes are required for export of ESAT-6/CFP-10 and for virulence of *Mycobacterium tuberculosis*. *Mol. Microbiol.* **51**, 359–370 (2004).

MICROBIOLOGY

Osman et al.
The C terminus of the mycobacterium ESX-1 secretion system substrate ESAT-6 is required for phagosomal membrane damage and virulence

PNAS | 9 of 9
https://doi.org/10.1073/pnas.2122161119